Biochemical Pharmacology 91 (2014) 323–336

Contents lists available at ScienceDirect

Biochemical Pharmacology

journal homepage: www.elsevier.com/locate/biochempharm

Trimetazidine prevents palmitate-induced mitochondrial fission and dysfunction in cultured cardiomyocytes

Jovan Kuzmicic [a,b], Valentina Parra [a,b,c], Hugo E. Verdejo [a,d], Camila López-Crisosto [a,b], Mario Chiong [a,b], Lorena García [a,b], Michael D. Jensen [e], David A. Bernlohr [f], Pablo F. Castro [a,d,*], Sergio Lavandero [a,b,c,*]

[a] Advanced Center for Chronic Diseases (ACCDiS), Universidad de Chile & Pontificia Universidad Católica de Chile, Santiago, Chile
[b] Centro Estudios Moleculares de la Célula, Facultad Ciencias Químicas y Farmacéuticas & Facultad de Medicina, Universidad de Chile, Santiago, Chile
[c] Department of Internal Medicine (Cardiology), University of Texas Southwestern Medical Center, Dallas, TX, USA
[d] División de Enfermedades Cardiovasculares, Facultad de Medicina, Pontificia Universidad Católica de Chile, Santiago, Chile
[e] Endocrine Research Unit, Mayo Clinic, Rochester, MN, USA
[f] Department of Biochemistry, Molecular Biology and Biophysics, University of Minnesota, Minneapolis, MN, USA

ARTICLE INFO

Article history:
Received 4 May 2014
Accepted 25 July 2014
Available online 1 August 2014

Chemical compounds studied in this article:
Trimetazidine CID 21109
Sodium palmitate CID 2735111

Keywords:
Cardiomyocyte
Trimetazidine
Palmitate
Mitochondrial dynamics
Metabolism

ABSTRACT

Metabolic and cardiovascular disease patients have increased plasma levels of lipids and, specifically, of palmitate, which can be toxic for several tissues. Trimetazidine (TMZ), a partial inhibitor of lipid oxidation, has been proposed as a metabolic modulator for several cardiovascular pathologies. However, its mechanism of action is controversial. Given the fact that TMZ is able to alter mitochondrial metabolism, we evaluated the protective role of TMZ on mitochondrial morphology and function in an *in vitro* model of lipotoxicity induced by palmitate. We treated cultured rat cardiomyocytes with BSA-conjugated palmitate (25 nM free), TMZ (0.1–100 μM), or a combination of both. We evaluated mitochondrial morphology and lipid accumulation by confocal fluorescence microscopy, parameters of mitochondrial metabolism (mitochondrial membrane potential, oxygen consumption rate [OCR], and ATP levels), and ceramide production by mass spectrometry and indirect immunofluorescence. Palmitate promoted mitochondrial fission evidenced by a decrease in mitochondrial volume (50%) and an increase in the number of mitochondria per cell (80%), whereas TMZ increased mitochondrial volume (39%), and decreased mitochondrial number (56%), suggesting mitochondrial fusion. Palmitate also decreased mitochondrial metabolism (ATP levels and OCR), while TMZ potentiated all the metabolic parameters assessed. Moreover, pretreatment with TMZ protected the cardiomyocytes from palmitate-induced mitochondrial fission and dysfunction. TMZ also increased lipid accumulation in cardiomyocytes, and prevented palmitate-induced ceramide production. Our data show that TMZ protects cardiomyocytes by changing intracellular lipid management. Thus, the beneficial effects of TMZ on patients with different cardiovascular pathologies can be related to modulation of the mitochondrial morphology and function.

1. Introduction

Metabolic syndrome and obesity are characterized by imbalanced caloric intake and expenditure, increasing the risk of diabetes and cardiovascular diseases, including heart failure [1]. Obese, diabetic and heart failure patients have increased plasma free fatty acids [2], which can elicit toxic effects (lipotoxicity) leading to cell death in several models, including cardiomyocytes [3]. Although the specific mechanism for lipotoxicity is not fully understood, sphingolipids may play a role because palmitate, the most abundant saturated free fatty acid, is the obligate substrate for initiating *de novo* ceramide synthesis [4]. We have shown that ceramides induce mitochondrial fission and cell death [5] by altering mitochondrial function and Ca^{2+} buffering capacity [6] in cultured cardiomyocytes. Interestingly, chemical inhibition of

* Corresponding authors at: Advanced Center for Chronic Diseases (ACCDiS), Facultad Ciencias Químicas y Farmacéuticas, Universidad de Chile, Olivos 1007, Santiago 8380492, Chile. Tel.: +56 229782903.
E-mail addresses: pcastro@med.puc.cl (P.F. Castro), slavander@uchile.cl (S. Lavandero).

http://dx.doi.org/10.1016/j.bcp.2014.07.022
0006-2952/

ceramide synthesis protects adult cardiomyocytes from palmitate-induced apoptosis [7].

Mitochondrial dynamics control mitochondrial shape and function by coordinating the opposing processes of mitochondrial fusion and fission [8,9]. Recent evidence suggests a role for mitochondrial dynamics in lipotoxicity [10,11]. In pancreatic β-cells, a complex mixture of free fatty acids (including palmitate) caused apoptosis [10], and in skeletal muscle palmitate induced mitochondrial dysfunction and insulin resistance [11]. Interestingly, in both studies the prevention of mitochondrial fission protected the cells from damage. In cardiomyocytes, lipotoxicity has been partially addressed but the role of mitochondrial dynamics in this process is unknown.

The heart uses different metabolic substrates to fuel the contractile machinery, and the importance of this energetic balance in the myocardium becomes particularly evident during heart failure [2]. Trimetazidine (TMZ), an antianginal drug used in Europe and Asia, has been proposed as a metabolic modulator for heart failure treatment. TMZ decreases free fatty acid-oxidation probably by partial inhibition of the β-oxidation enzyme long chain 3-ketoacyl-CoA thiolase (3-CAT) [12], and carnitine-palmitoyl-transferase 1 (CPT1) [13], thereby increasing glucose utilization for ATP production [14]. At the mitochondrial level, TMZ decreases the activity of complex I of the electron transport chain during ischemia [15], decreasing oxygen consumption, production of reactive oxygen species (ROS) [16] and preserving mitochondrial integrity [17], allowing conservation of mitochondrial membrane potential (Ψ_{mt}) [18], thus preventing the opening of the mitochondrial permeability transition pore [19] and apoptosis [20].

Lipotoxicity is linked to mitochondrial dysfunction and ROS production [21], sharing some of the features of ischemic damage. Because diabetes, heart failure, and other cardiac pathologies are associated with increased plasma free fatty acids and cardiac lipotoxicity [1], we sought to evaluate the protective effect of TMZ on palmitate lipotoxicity using a cultured cardiomyocyte model system. We evaluated changes in mitochondrial morphology, metabolism, and ceramide production. To our knowledge, this corresponds to the first report of protective effects of TMZ on palmitate-induced lipotoxicity in cardiomyocytes, thus expanding our understanding of its mechanism of action [22].

2. Materials and methods

2.1. Materials

Antibodies against DRP-1 and HSP70 were from BD Biosciences and Affinity BioReagents, respectively. Antibodies for MFN-2 and OPA-1 were from Abcam. Antibodies against C16-ceramide and FIS-1 were from Enzo Life Sciences. Tetramethylrhodamine-methyl-ester (TMRM), mitotracker Green-FM (MTG), HCS-LipidTOX Green, Hoechst 33342, the antibodies Alexa-543 conjugated anti-mouse IgG and Alexa-488 conjugated anti-rabbit IgG, 5-(and-6)-chloromethyl-2′,7′-dichlorodihydrofluorescein diacetate acetyl ester (CM-H2DCFDA), essentially fatty-acid-free BSA and FBS were from Invitrogen. Sodium palmitate was purchased from Nu-Chek Prep Inc. Anti-caspase-3 rabbit antibody was from Cell Signaling. Anti-β-tubulin antibody, propidium iodide (PI), carbonyl cyanide m-chlorophenyl-hydrazone (CCCP), Dulbecco's modified Eagle's medium (DMEM), M199 medium, and other reagents were from Sigma–Aldrich Corp. Protein assay reagents were from Bio-Rad.

2.2. Cardiomyocyte isolation

Cardiomyocytes were isolated from neonatal Sprague–Dawley rats as previously described [5,23,24]. Briefly, 2–3 days old pups were sacrificed by decapitation, and the hearts extracted under sterile conditions, carefully minced, and digested with type-II collagenase and pancreatine (37 °C). After digestion, cells were collected and the cardiomyocytes separated from fibroblasts before seeding.

Rats were kept at the institutional animal breeding facility. All studies were performed according to the NIH Guide for the Care and Use of Laboratory Animals (NIH Publication No. 85-23, revised 1996) and approved by our Institutional Ethics Committee.

2.3. Cell culture

Cells were maintained in DME:M199 (4:1) medium supplemented with 5% FBS and plated at final density of 1–8 $\times$ 10^3/mm^2 on gelatin-coated 35-, 60-mm or 12-, 96-well Petri dishes according to experimental design. For microscopy experiments, cells were plated on gelatin-coated glass coverslips. Cells were left untouched for 24 h after seeding, then the media was changed every day and cell were cultured in DMEM:M199 (4:1) medium supplemented with 5% FBS until needed. Sodium palmitate was added to culture media containing fatty-acid-free BSA in a ratio of 3.3:1 and allowed to conjugate for 30 min at 37 °C. An equivalent concentration of 500 μM [25] was used, giving an final concentration of 25 nM free palmitate [26]. TMZ was dissolved in water and added at concentrations ranging between 0.1 and 100 μM.

2.4. Mitochondrial morphology analysis

Procedure was performed as previously described [5,6,23]. Briefly, mitochondria were stained with Mitotracker green (400 nM, 30 min) in Krebs solution (containing [in mM]: 145 NaCl; 5 KCl; 1 EGTA; 1 $MgCl_2$; 10 HEPES-Na; 5.6 glucose; pH 7.4) at 37 °C. Confocal Z-stack images were obtained with a Carl Zeiss LSM-5 Pascal 5 Axiovert 200 microscope, using the LSM 5 3.2 image capture and analysis software, and a Plan-Apochromat 63×/1.4 Oil DIC objective. Images were processed and analyzed using the ImageJ software. Z-stacks were 3D reconstructed and the number of mitochondria and their individual volume were quantified using the VolumeJ plug-in for ImageJ. The sum of individual mitochondrial volume and the mitochondrial number was used to calculate the "mean mitochondrial volume", an indicator of mitochondrial volume used for comparisons. Additionally, the percentage of cells showing a fragmented mitochondria pattern was determined manually. Thus, an increase in fragmented appearance and mitochondrial number, together with a decrease in mean mitochondrial volume were considered as a fission criteria. The opposite was considered for fusion [5,6,23]. Each experiment was performed at least three independent times and 16–25 cells were analyzed per condition.

2.5. Immunofluorescence staining

Cells were fixed with 4% paraformaldehyde and permeabilized with 0.1% Triton X-100 in ice-cold PBS. Cells were incubated with primary antibodies against DPR-1 (1:500) and FIS-1 (1:500). Secondary antibodies were anti-mouse Alexa-543 and anti-rabbit Alexa-488 (1:1000). Effective colocalization was determined using the Mander's Coefficient as previously described [5,27].

2.6. Mitochondrial membrane potential and ROS determination

Mitochondrial membrane potential (Ψ_{mt}) and ROS were measured with TMRM (200 nM, 30 min) or CM-H2DCFDA (10 μM, 30 min), respectively. Mean population fluorescence

was measured by flow cytometry using a FACScan system (Becton–Dickinson). CCCP or H_2O_2 were used as positive control for Ψ_{mt} loss or ROS, respectively. Data were analyzed using the Cell Quest (BD) software.

2.7. Cellular respiration

Cells were suspended in PBS in a sealed chamber (25 °C) coupled to a 5331 Clark electrode (Yellow Springs Instruments). Oxygen consumption rates (OCR) were calculated over a 5–10 min period. CCCP (200 nM) and oligomycin (500 nM) were added to obtain maximal respiration and proton leak, respectively. Respiration rates were normalized to controls [23]. As a second method, oxygen consumption was also measured using a fluorescence-based oxygen sensor (NeoFox, Ocean Optics) connected to a phase measurement system from the same company. The sensor was calibrated according to the manufacturer's instructions.

2.8. ATP measurement

Intracellular ATP levels were determined with a luciferin/luciferase based ATP detection kit CellTiter-Glo Luminiscent Cell Viability Assay (Promega) according to the manufacturer's instructions. Sample luminescence was quantified in a TopCount NXT microplate luminescence counter (Perkin-Elmer, Waltham, MA). Data was normalized as fold over control.

2.9. Cell death determination

A flow cytometry-based assay and a luminescence-based kit were employed to assess necrosis. To determine cell viability, cardiomyocytes were suspended and incubated with PI (15 mM) prior to flow cytometry [6]. Dye incorporation depends on membrane stability, thus increased fluorescence acts as an indicator of increased necrosis [6]. H_2O_2 (175 mM, 30 min) was used as positive control. Furthermore, a commercial kit for assessing lactate dehydrogenase (LDH) release (Promega CytoTox96®) was employed following the manufacturers' indications [28,29]. In order to measure apoptosis, a flow cytometry-based assay and an indirect measurement of caspase-3 activity were performed. DNA fragmentation was assessed in cells permeabilized with methanol overnight (−20 °C), treated with RNase and analyzed by flow cytometry with PI dye (40 mM) [6]. In this condition, permeabilization ensures access of the dye to the DNA of every cell in the sample thus changes in fluorescence intensity reflect changes in the cellular content of DNA. Therefore, an increase on the population of lower intensity than the highest peak (G1 population) corresponds to the SubG1 population and represents increased DNA fragmentation and apoptosis [6].

2.10. Neutral lipid staining

Intracellular lipid droplets were stained with HCS LipidTOX Green as indicated by the manufacturer. Briefly, cells were fixed with 4% paraformaldehyde in PBS containing Hoechst (0.5 μg/ml). Lipid droplets were stained in PBS using the 1000× HSC LipidTox working solution provided for at least 30 min and observed directly (no washing) under a Carl Zeiss LSM-5 Pascal 5 Axiovert 200 confocal microscope with a Plan-Apochromat 63×/1.4 Oil DIC objective. The number of lipid droplets and lipid droplet area per cell were determined in the raw images. Due to the low lipid accumulation capability of cardiomyocytes, the analysis was performed only in dye-positive cells that showed at least one lipid droplet (approximately 40% of cells), defined as an object with an area bigger than 10 pixels^2.

2.11. Sphingolipid determination

The cellular content of sphingolipids was measured using a UPLC/MS/MS approach in whole cell extracts as previously described [30,31]. Briefly, cells were collected by trypsinization, washed with ice-cold PBS, centrifuged, and the dry pellet was flash-frozen in liquid nitrogen and stored at −80 °C until analysis. Pellets were thawed, homogenized (buffer [in mM]: 250 sucrose, 25 KCl, 50 Tris, and 0.5 EDTA, pH 7.4), and supplemented with an internal standard solution (17C-sphingosine and 17C-S1P, and 17C16-Cer Avanti Polar Lipids). The mixture was extracted twice, evaporated under nitrogen flow, and reconstituted in 100 μl of LC Solvent A (2 mM NH_4HCO_2, 0.15% HCOOH in methanol) for UPLC/MS/MS analysis on a Waters Acquity UPLC system coupled with Thermo TSQ Quantum Ultra mass spectrometer. The results were expressed as sphingolipid content per μg of protein in the sample. Additionally, we assessed the production of intracellular ceramides by indirect immunofluorescence using an antibody that detects C-16 ceramide forms. Cells were prepared as described in Section 2.5, and stained using a primary antibody against C16-ceramide (1:100). Samples were visualized under a confocal microscope. Total fluorescence was normalized to cell area before comparison.

2.12. Western blotting

Proteins were separated by SDS–PAGE and electrotransferred to nitrocellulose. Membranes were blocked for unspecific binding with 5% non-fat milk in Tris-buffered saline containing 0.1% (v/v) Tween 20 (TBST). Membranes were blotted with primary antibodies (1:1000) at 4 °C overnight and incubated with secondary antibodies linked to horseradish peroxidase (1:5000). Bands were detected using ECL with exposure to Kodak film and quantified by scanning densitometry. Protein content was normalized to β-tubulin expression.

2.13. DRP-1 immunoprecipitation

Immunoprecipitation of DRP-1 was performed overnight using 2 μg of anti-DRP-1 antibody (Santa Cruz) on 600 μg of total protein. DRP-1 was precipitated with Sepharose beads conjugated to protein G (Santa Cruz), resolved by SDS–PAGE and phosphorylation was assessed with an anti-phospho-DRP-1 antibody (Cell Signaling, 1:2000).

2.14. Statistical analysis

Data are shown as mean ± SEM of the number of independent experiments indicated (n) or as a representative data of experiments performed on at least three separate occasions with similar outcomes. Univariate data comparisons were made by one-way ANOVA followed by Dunnett or Tuckey tests as indicated. Statistical significance was defined as $P < 0.05$.

3. Results

3.1. Palmitate induces mitochondrial fission in cardiomyocytes

Several reports have shown toxic effects of palmitate, ranging from mitochondrial fragmentation and dysfunction [11] to cell death [3,7]. However, the underlying mechanism is not fully understood, and as such, we sought to evaluate whether palmitate alters mitochondrial morphology and function in our conditions. Fig. 1A shows mitochondrial fission caused by palmitate, evidenced by a significant increase in the percentage of cells with

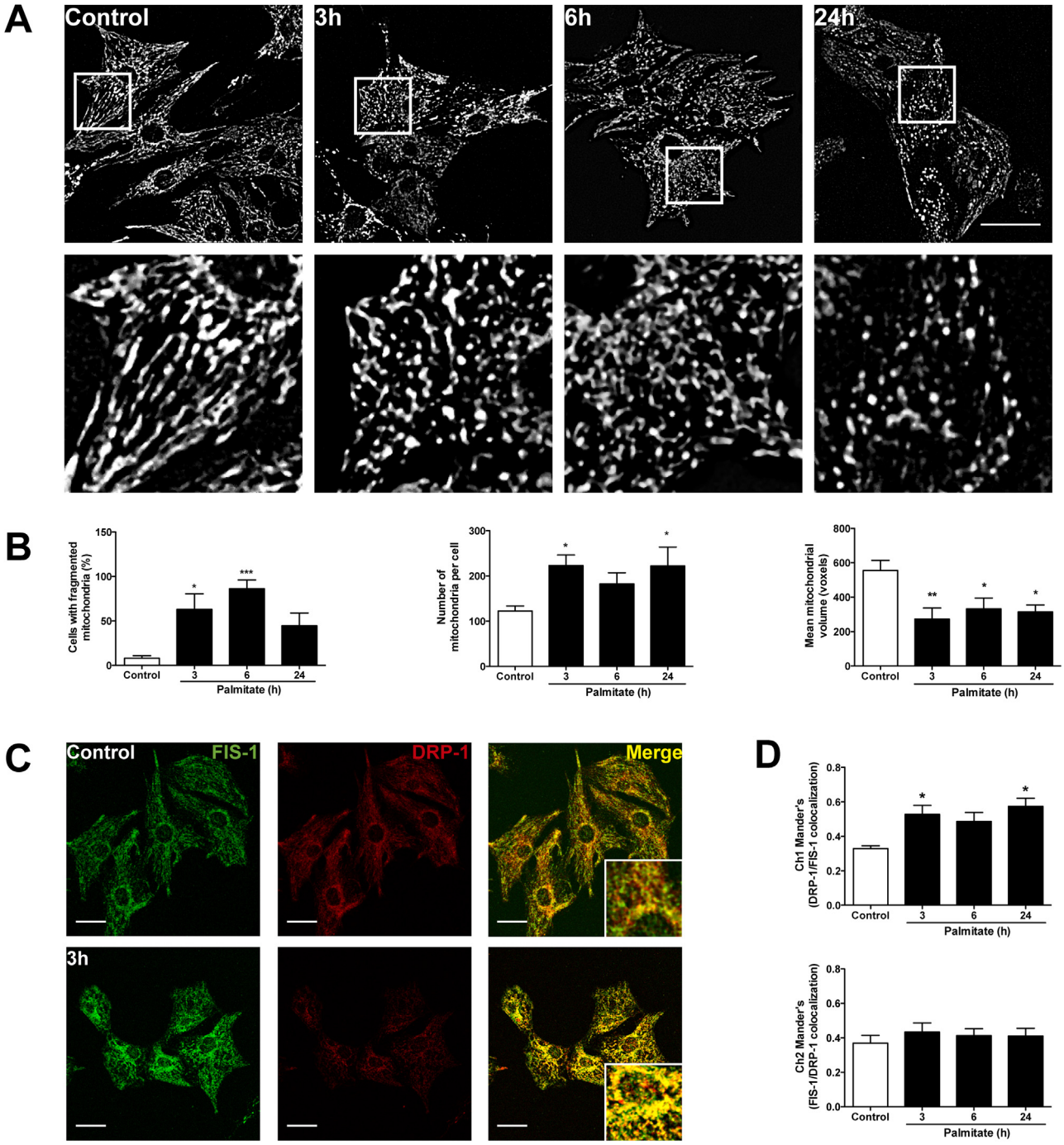

Fig. 1. Palmitate treatment induces mitochondrial fission. Cells were treated with palmitate (25 nM free, 0–24 h). A, Representative images of Mitotracker-Green-stained mitochondria (400 nM, 30 min) observed under a confocal microscope. Scale bar: 20 μm. B, Percentage of cells showing a fragmented-mitochondria pattern (left), number of mitochondria per cell (middle) and mean mitochondrial volume (right) were quantified ($n = 6$). C, Representative images of control and palmitate treated (3 h) cells immunostained for FIS-1 (green, left), DRP-1 (red, middle) and merge (yellow, right). Scale bar: 20 μm. D, Colocalization was quantified using Mander's coefficient for DRP-1 to FIS-1 (upper panel) and FIS-1 to DRP-1 (lower panel) at all time points (0–24 h, $n = 3$). $^{*}P < 0.05$; $^{**}P < 0.01$; $^{***}P < 0.001$ vs. control. Data were analyzed by Dunnette's following 1-way ANOVA. Bar graphs represent mean ± SEM. (For interpretation of the references to color in this figure legend, the reader is referred to the web version of the article.)

fragmented appearance and the number of mitochondria per cell, accompanied by a significant reduction in mean mitochondrial volume (Fig. 1B). This phenotype was established at 3 h of treatment and persisted until 24 h. Since mitochondrial morphology depends on the balance between mitochondrial fission and fusion [8,9], the participation of the mitochondrial fission machinery in palmitate treated cells was evaluated. We analyzed colocalization of the fission proteins DRP-1 and FIS-1 by indirect immunofluorescence. Palmitate significantly increased the effective colocalization of DRP-1 to FIS-1 (Fig. 1C and D), whereas no significant changes were observed for FIS-1 over DRP-1 as we have previously reported [5]. To further explore the participation of the mitochondria-shaping machinery, we performed Western blots of the fission proteins DRP-1 and FIS-1, and the non-related mitochondrial protein HSP70 as a marker of mitochondrial mass (Fig. 2A and B). We observed no changes in any of these markers, or

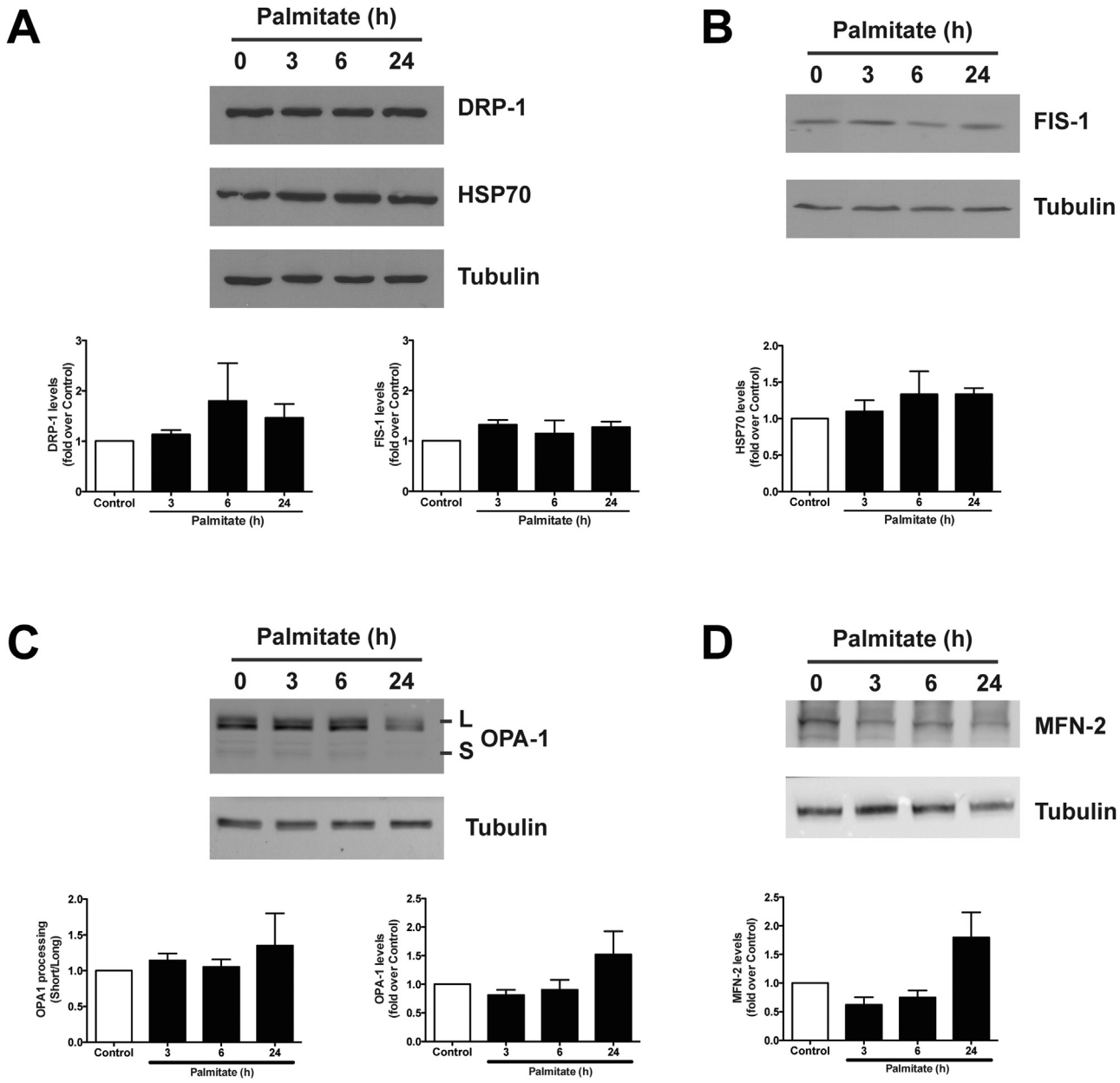

Fig. 2. Palmitate does not alter the expression of the mitochondrial dynamics proteins. Cells were treated with palmitate (25 nM) for the indicated times and then total protein extracts were collected. Representative Western blots and quantifications for the fission proteins DRP-1 (A) and FIS-1 (B), the fusion proteins OPA-1 (C) and MFN-2 (D) ($n = 4$) are shown. Also the non-related mitochondrial protein HSP70 (A) is shown ($n = 4$). Bar graphs represent mean ± SEM.

in the levels of the fusion proteins OPA-1 and MFN-2 (Fig. 2C and D). Taken together, these data suggest that palmitate induces mitochondrial fragmentation by promoting the translocation of the fission protein DPR-1 to the mitochondria.

3.2. Palmitate causes mitochondrial dysfunction at early time points

Prior to studying the effects of palmitate on mitochondrial metabolism, we evaluated cell death in our conditions since palmitate has been widely described to affect cell survival in previous studies [3,32]. To this end, we first performed rough measurements of necrosis and apoptosis, using flow cytometry-based techniques, and found evidence of cell death at 24 h without changes at shorter times (Fig. 3A and B). To further characterize the type of cell death observed we measured specific markers for necrotic and apoptotic death. As shown in Fig. 3C, palmitate treatment significantly increased the release of LDH, a necrosis marker, at 24 h only. Similarly, Fig. 3D indicates that cleaved caspase-3 can be observed at 6 and 24 h, but only at later time points it reached expression levels comparable to sorbitol treatment, a known inductor of apoptosis in our model [33]. Taken together, these data suggest that palmitate induced necrotic and apoptotic cell death, but only at 24 h of treatment. Thus, the morphological effects described above were not due to increased cell death at early time points. In order to avoid interference, we next evaluated the metabolic parameters at 3 h of palmitate treatment, a time sufficient to induce mitochondrial fission without induction of cell death. We evaluated mitochondrial membrane potential (Ψ_{mt}), intracellular ATP, cellular oxygen consumption rate (OCR) and total ROS levels (Fig. 4). Palmitate induced a significant decrease in the intracellular ATP levels, accompanied by a diminished OCR under basal and maximal (uncoupled) respiration conditions. However, Ψ_{mt} only decreased after 24 h post treatment (without any changes at shorter times),

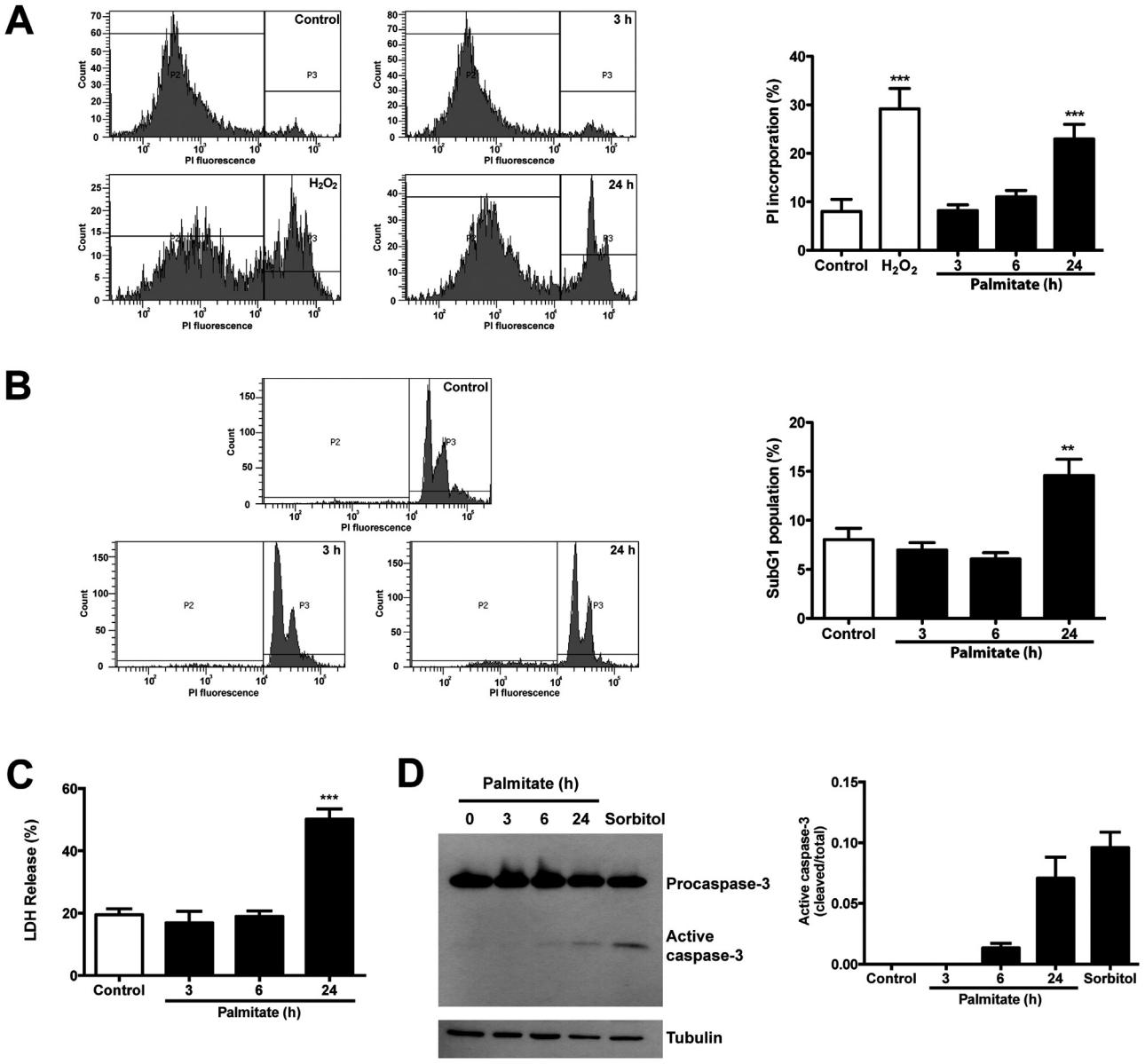

Fig. 3. Palmitate induces cardiomyocyte death at long incubation times. A, Cell viability was determined by PI incorporation on intact cells and analyzed by flow cytometry. Representative histograms of the live (P2) and dead (P3) populations for control, palmitate-treated cells (25 nM) and cells treated with H_2O_2 (175 mM, 30 min) as positive control ($n = 4$). B, DNA laddering (SubG1 population) on permeabilized cells stained with PI was measured by flow cytometry as a marker of apoptosis. Representative histograms of the DNA fragmentation are shown for control and palmitate-treated cells (25 nM, $n = 4$). C, LDH release was measured in palmitate-treated cells (25 nM) using a colorimetric-based commercial kit ($n = 3$). D, Cleaved caspase-3 was detected by Western blot. A representative blot (left panel) and quantification (right panel) are shown ($n = 5$). Data points without bars were below detection level. Sorbitol (300 mM, 6 h) was used as positive control for apoptosis. $^{**}P < 0.01$; $^{***}P < 0.001$ vs. control. Dunnette's post 1-way ANOVA. Bar graphs represent mean ± SEM.

which can be highly influenced by the cell death process occurring under palmitate stimulation at longer time points. Although, a decrease in Ψ_{mt} would be expected to accompany the decrease in OCR and ATP levels at 3 h, we did not observe it. This result is not surprising considering the fact that mitochondrial membrane potential is around +150 mV, and very close to equilibrium in the close microenvironment of the mitochondria, which offers a pH gradient of −0.5 pH units (30 mV) [34]. This means that only a slight change in mitochondrial potential is needed to cause a significant impact on OCR. In this same context, the measurement of Ψ_{mt} with TMRM can be not sensitive enough to detect the small changes that can also be affecting mitochondrial dynamics [35,36]. Finally, and similar to previous reports [3], we did not observe changes in ROS production with palmitate (Fig. 4D). Taken together, these results suggest that palmitate induces mitochondrial dysfunction parallel to mitochondrial fission and previous to cell death.

3.3. TMZ induces mitochondrial fusion in cardiomyocytes

Because TMZ may be a metabolic modulator in patients with lipid handling alterations [37], and the controversy of its action mechanism [22], we sought to evaluate its effects in our lipotoxicity model. We first characterized TMZ effects alone, and show in Fig. 5A that low TMZ concentrations induced mitochondrial fusion, evidenced by a significant decrease in the number of mitochondria per cell with increased mean mitochondrial volume (Fig. 5B) after 24 h of treatment. Interestingly, using a higher concentration of TMZ (100 μM) we observed an increase in the number of mitochondria per cell (Fig. 5B), suggesting a reversion of

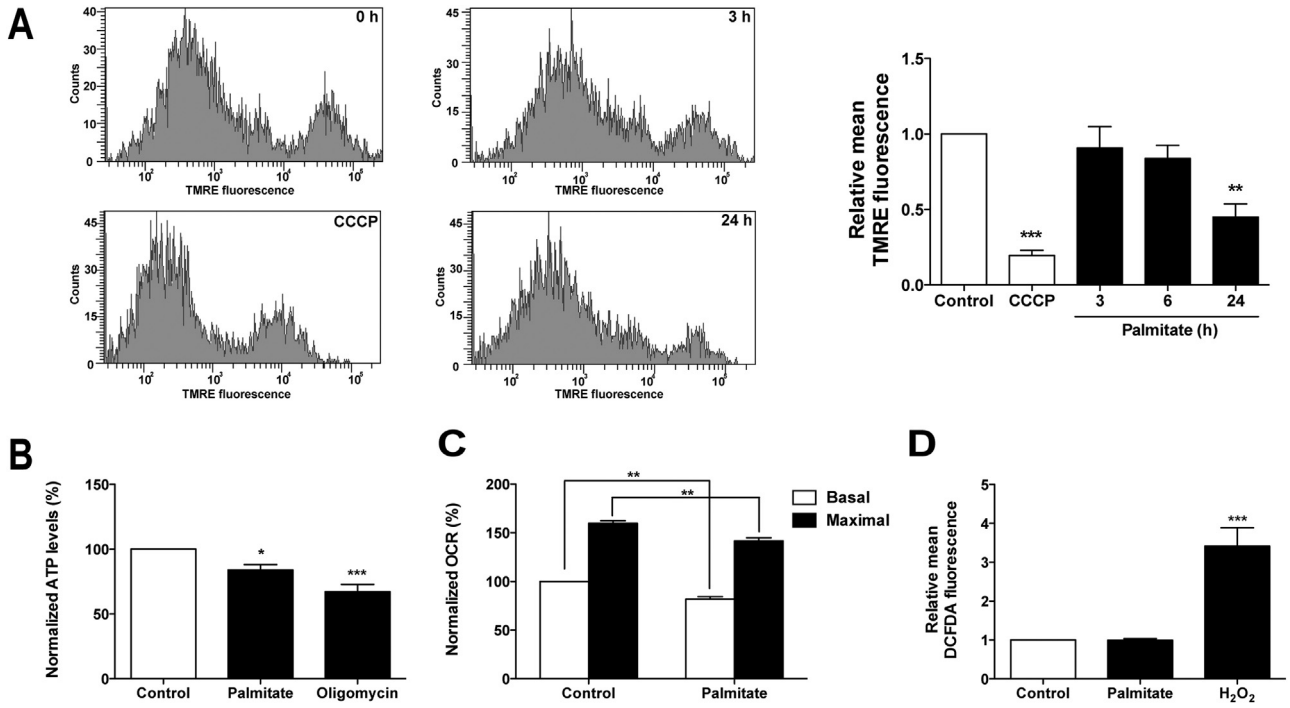

Fig. 4. Palmitate treatment decreases metabolic parameters. A, Mitochondrial membrane potential was determined by TMRM staining (200 nM, 30 min) and flow cytometry. The uncoupler CCCP (10 μM) was used as positive control for mitochondrial depolarization. Representative histograms (left) and quantifications (right) are shown for control (0 h), palmitate-treated (25 nM, 3–24 h) and CCCP-treated cells ($n = 4$). B, Intracellular ATP was measured in palmitate-treated cells (25 nM free, 3 h) with a commercial kit. Oligomicyn (10 μM, 1 h) is shown as a positive control for ATP drop ($n = 6$). C, Oxygen consumption rates were measured in basal and maximal (uncoupled) conditions for control and palmitate-treated (3 h) cells using a Clark's electrode ($n = 3$). D, Total cell reactive oxygen species (ROS) levels were measured by flow cytometry using CM-H2DCFDA dye ($n = 4$). H_2O_2 was used as ROS positive control. $^*P < 0.05$; $^{**}P < 0.01$; $^{***}P < 0.001$ vs. control. Data were analyzed by Dunnette's following 1-way ANOVA. Bar graphs represent mean ± SEM.

the phenotype. To further explore the effects of TMZ, we evaluated the expression levels of the mitochondrial fusion proteins OPA-1 (Fig. 5C) and MFN-2 (Fig. 5D), the non-related protein HSP70 (Fig. 5E) and the fission proteins DRP-1 and FIS-1 (Fig. 3F). We did not observe changes in the abundance of any of these proteins at any of the TMZ concentrations evaluated. However, changes in the activity of any of these proteins due to post-translational modifications cannot be excluded.

3.4. TMZ potentiates mitochondrial metabolism

To further describe TMZ effects, we studied mitochondrial metabolism by measuring the aforementioned parameters (Ψ_{mt}, ATP levels, OCR, and ROS). Consistent with the morphologic data (Fig. 5), 1 μM TMZ increased Ψ_{mt} (Fig. 6A), intracellular ATP levels (Fig. 6B), and both basal (Fig. 6C) and maximal OCR (Fig. 6D). The higher concentration (100 μM), TMZ showed no changes relative to the controls in any of these parameters. To deepen our understanding of this metabolic potentiation, we also evaluated oligomycin-insensitive OCR (proton leak, Fig. 6E) and ROS levels (Fig. 6F) with 1 μM TMZ. We found no significant differences in either of these parameters, suggesting that the rise in basal and maximal OCR result from increased mitochondrial activity. Additionally, no changes in cell viability were observed in any of the TMZ treatment conditions (data not shown). Taken together, the results in Figs. 5 and 6 suggest that a low concentration of TMZ induces mitochondrial fusion and potentiates mitochondrial metabolism.

3.5. TMZ protects cardiomyocytes from palmitate-induced mitochondrial fission and dysfunction

Considering the positive effects of TMZ on mitochondrial function and morphology, we decided to test if TMZ could protect cardiomyocytes from palmitate-induced lipotoxicity. To account for the time-lapse differences of TMZ and palmitate effects, cells were pre-incubated with or without TMZ (1 μM, 24 h) and then exposed to palmitate (3 h). We analyzed mitochondrial morphology and metabolism. As described previously, palmitate induced marked mitochondrial fission (Fig. 1), while TMZ alone had the opposite effects (Fig. 5). Interestingly, pre-incubation with TMZ (24 h) completely blunted palmitate effects and protected cells from altered mitochondrial morphology (Fig. 7A and B). To explore the mechanism of this protection, we assessed DRP-1 phosphorylation state on Ser637, an inactivating phosphorylation site, by immunoprecipitation [38]. Palmitate decreased DRP-1 phosphorylation, consistent with increased mitochondrial fission through DRP-1 activity (Fig. 1C), while TMZ prevented this effect (Fig. 7C). When assessing mitochondrial metabolism, we found that TMZ protected the cells from palmitate-induced ATP drop (Fig. 7D), and both basal (Fig. 7E) and maximal OCR (Fig. 7F) reduction. In order to further support these findings, we also included a secondary experimental approach for OCR determination by using a fluorescent oxygen probe. As shown in Fig. 7G and H, OCR reduction by palmitate was also found to be prevented with TMZ. Collectively, these results suggest that TMZ protects from palmitate lipotoxicity by preserving mitochondrial integrity and function.

To further characterize TMZ protective effects, we assessed the possible intracellular fates of palmitate in the presence of TMZ. First, we evaluated if TMZ alters the balance between lipid usage and storage in cardiomyocytes. For this, we stained fixed cells with the neutral-lipid specific dye LipidTOX and observed them under a confocal microscope. As expected, control cells show few lipid droplets, which were not affected by palmitate treatment (Fig. 8A), consistent with the notion that palmitate is poorly incorporated into fatty acid storage. Interestingly, TMZ alone greatly increased

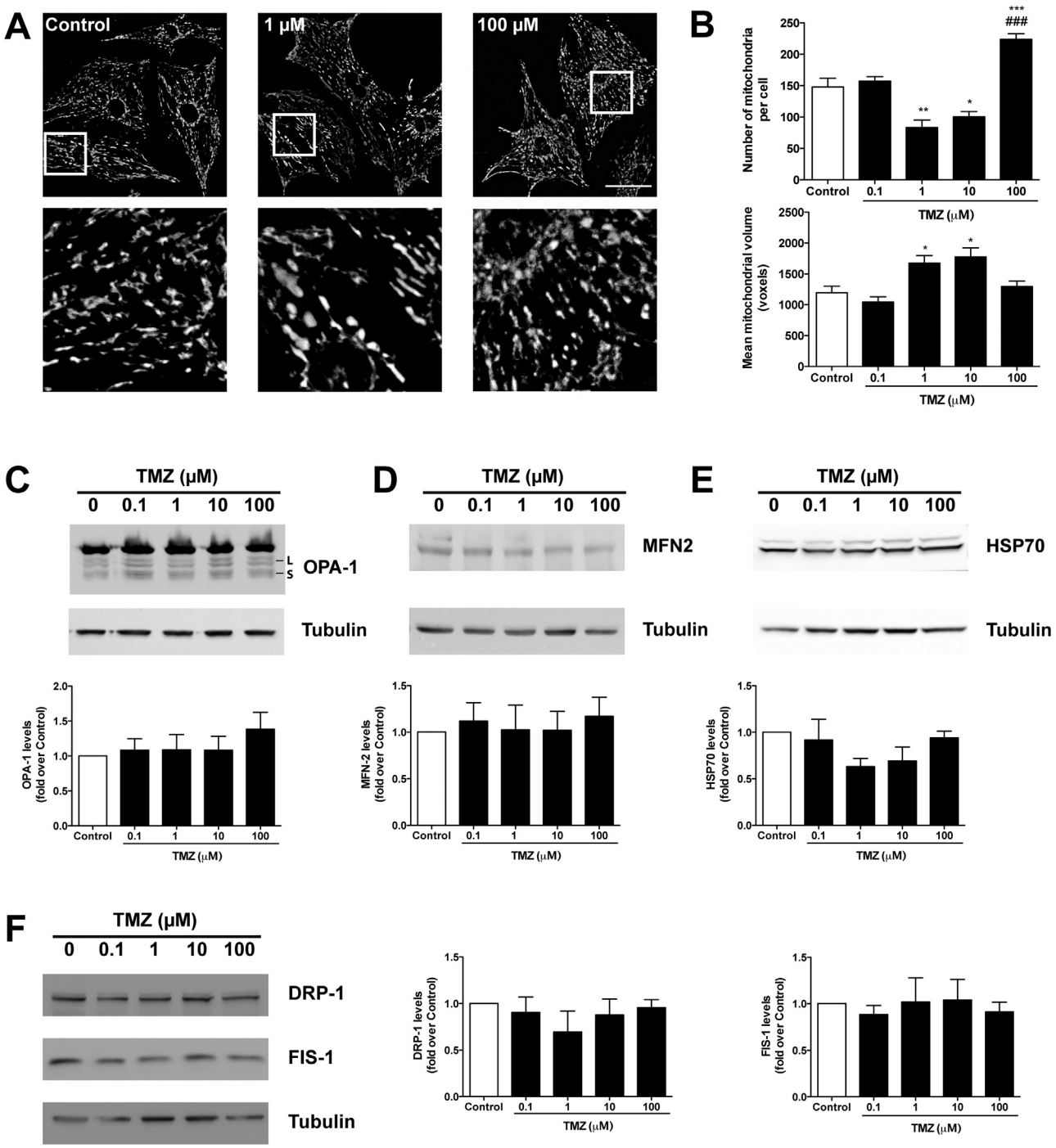

Fig. 5. TMZ induces mitochondrial fusion at low concentrations. Cells were treated with TMZ (0–100 μM) for 24 h. A, Representative images of Mitotracker-Green-stained mitochondria (400 nM, 30 min) observed under a confocal microscope. Scale bar: 10 μm. B, Number of mitochondria per cell (upper pannel) and mean mitochondrial volume were quantified (lower pannel). $^{*}P < 0.05$; $^{**}P < 0.01$; $^{***}P < 0.001$ vs. control. $^{\#\#\#}P < 0.001$ vs. 1 μM. Tuckey post 1-way ANOVA, $n = 5$. Representative Western blots for the fusion proteins OPA-1 (C) and MFN2 (D), the mitochondrial protein HSP70 (E), and the fission proteins DRP-1 and FIS-1 (F) and their quantifications are shown ($n = 3$). Bar graphs represent mean ± SEM.

the number and size of droplets compared to controls, and further increased the area of lipid droplet in the presence of palmitate (Fig. 8A), suggesting that TMZ acts favoring lipid accumulation. Considering that palmitate is a preferential substrate for *de novo* ceramide synthesis [4], we hypothesized that sequestering lipid excess into lipid droplets could reduce ceramide production. Accordingly, palmitate alone significantly increased sphinganine (SPA) and C16 ceramide (Fig. 8B) production, two key intermediates in the *de novo* ceramide synthesis pathway. The levels of the ceramide degradation intermediary, sphingosine (SPH), and the sphingolipid recycling metabolite, sphingosine 1-phosphate (S1P), were not changed (Fig. 6B), suggesting induction of *de novo* pathway in our conditions. To further explore the protection of TMZ from palmitate toxicity, we performed immunofluorescence analysis using a C16-specific antibody as ceramide production readout, since this ceramide form was more affected by palmitate treatment (no commercial antibody against SPA, SPH or S1P are currently available). As expected, palmitate treatment significantly

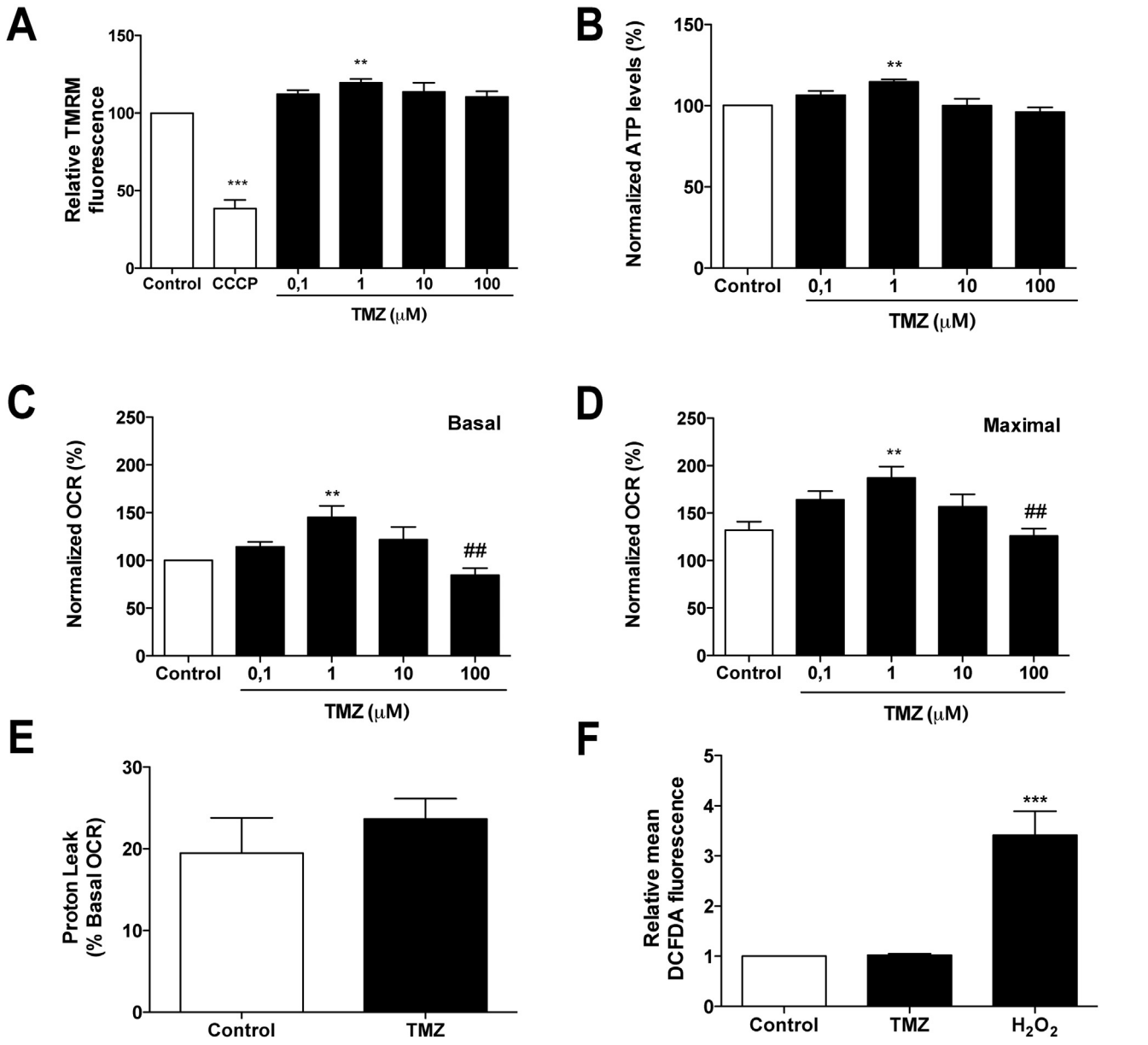

Fig. 6. TMZ increases metabolic parameters at low concentrations. Cells were treated with TMZ (0–100 μM) for 24 h. A, Mitochondrial membrane potential was determined by TMRM staining (200 nM, 30 min) and flow cytometry. CCCP is showed as a positive control for mitochondrial depolarization ($n = 5$). B, Intracellular ATP levels were measured with a commercial kit ($n = 6$). Basal (C) and maximal uncoupled (D) oxygen consumption rates were determined with a Clark electrode. Proton leak (oligomycin-insensitive) oxygen consumption rates (E) were measured in cells treated with 1 μM TMZ. ROS levels were determined by flow cytometry using CM-H2DCFDA dye (F). H_2O_2 was used as positive control for ROS. $^{**}P < 0.01$; $^{***}P < 0.001$ vs. Control. $^{\#\#}P < 0.01$ vs. 1 μM. Data were compared by Tuckey following 1-way ANOVA. Bar graphs represent mean ± SEM.

augmented ceramide production evidenced by increased total fluorescence to cell area ratio (Fig. 6C). This effect was completely blunted by TMZ treatment, while TMZ alone had no effects on ceramide production (Fig. 6C). These results suggest that TMZ redirects intracellular lipid destination protecting the cells by blocking the generation of toxic intermediates in conditions of lipid excess. To our knowledge, these data corresponds to the first description of TMZ effects on mitochondrial morphology and ceramide synthesis in cardiomyocytes, expanding the intracellular actions of this agent.

4. Discussion

The present study shows that palmitate induced mitochondrial fission and dysfunction in neonatal cardiomyocytes, which can be prevented by the β-oxidation inhibitor TMZ. Our data suggest that TMZ induces the accumulation of lipids into lipid droplets, thus sequestering the excess of palmitate in a metabolically neutral reservoir, hindering the production of ceramides. These results may expand our knowledge and comprehension of the action mechanism of TMZ, a matter that is still controversial.

Due to the elevated metabolic rate of cardiomyocytes, the possible relationship between mitochondrial dynamics, metabolism and cardiac mechanical efficiency has become an interesting subject of study. Our data show that palmitate induced mitochondrial fragmentation, by activating the mitochondrial fission protein DRP-1, and mitochondrial dysfunction in neonatal cardiomyocytes. In agreement with other studies [11,39], we did not observe changes in the fusion proteins MFN2 or OPA1 induced by palmitate. Recently, Jheng et al. [11] described that palmitate

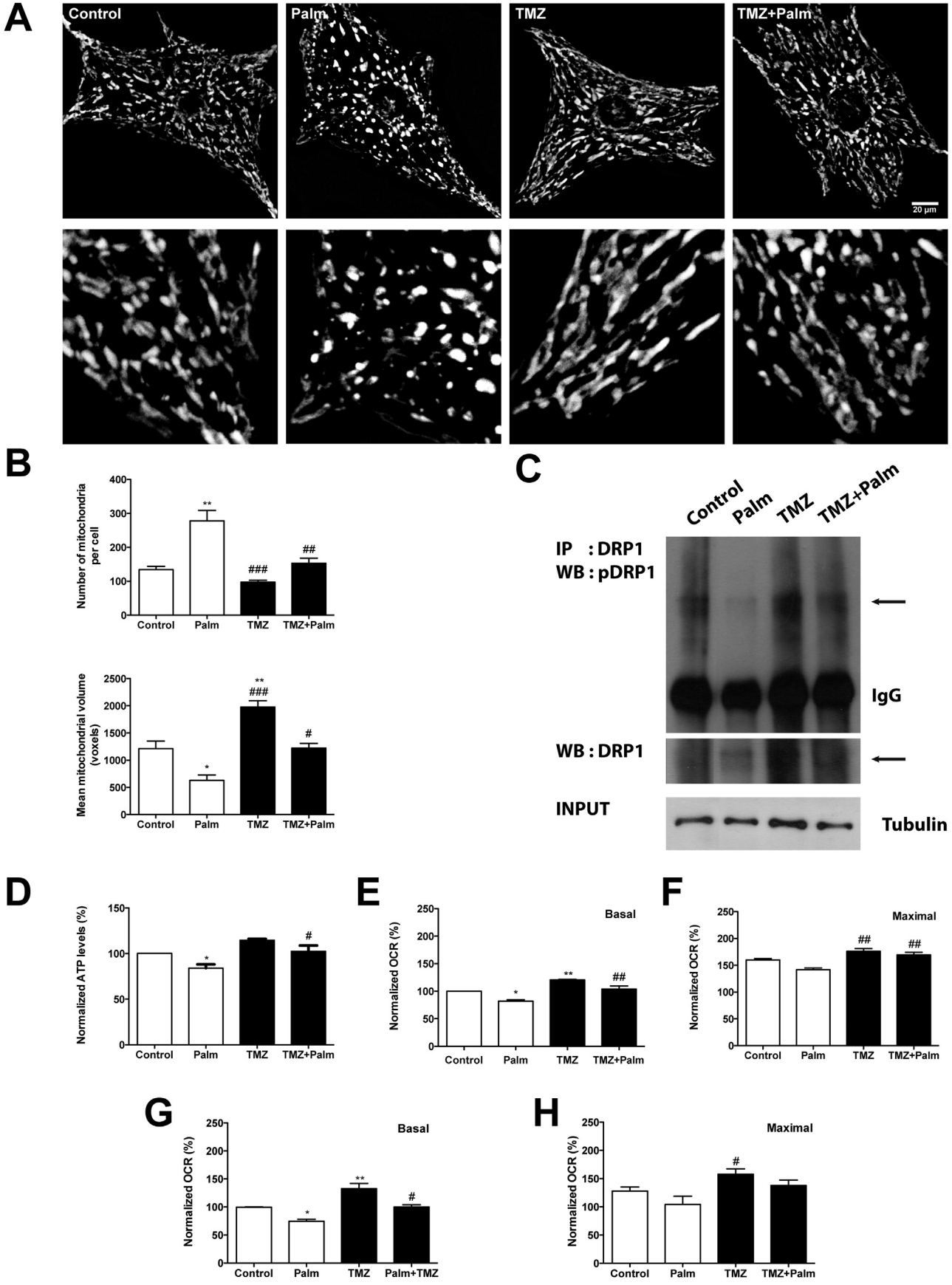

Fig. 7. TMZ at low concentrations protects cardiomyocytes from the morphological and metabolic effects of palmitate. A, Cells were stained with MTG (400 nM) and observed under a confocal microscope. Representative images and magnifications are showed for Control (left), palmitate- (middle left), TMZ- (middle right) and TMZ + palmitate-treated cells (right). Scale bar: 20 μm. (B) Number of mitochondria per cell (upper panel) and mean mitochondrial volume (lower panel) were quantified ($n = 3$).

toxicity is associated with mitochondrial fission and insulin resistance in skeletal muscle [11], effects that can be both prevented by inhibiting mitochondrial fission, specifically at DRP-1 level [11]. Similarly, our data show that palmitate-induced mitochondrial fission and dysfunction can be prevented when mitochondrial morphology is preserved by TMZ. Although the mechanism by which palmitate could activate mitochondrial fission was not determined, we show evidence of DRP-1 activation by decreased Ser637 phosphorylation. As mentioned above, DRP-1 phosphorylation is regulated by the antagonistic activities of PKA and calcineurin, which can reduce or increase DRP-1 fission activity, respectively [38]. Interestingly, cytosolic calcium levels can regulate calcineurin activity. Although we did not evaluate changes in calcium handling, it has been greatly described in β-cells that palmitate can rapidly increase cytosolic calcium levels by inducing calcium release from ER stores and extracellular Ca^{2+} influx [40,41]. Moreover, in isolated mitochondria there is evidence to support the existence of a mitochondrial cyclosporin A-insensitive pore that can be opened by palmitate. This pore leads to mitochondrial depolarization, swelling, and Ca^{2+} release, which can be prevented by Ca^{2+} uniporter inhibitors and Ca^{2+} chelators [42]. This evidence suggests that Ca^{2+} can play an important role in palmitate toxicity. Another possibility could be related to the production of lipid intermediaries from palmitate, which is a known preferential substrate for the *de novo* synthesis of ceramides [4]. In this line, our group has previously shown that ceramides induce mitochondrial fission in cardiomyocytes by activating the fission protein DRP-1 [5]. Similarly, it has been previously shown, by others and us, that ceramides decrease mitochondrial function and metabolic activity [4,6]. Interestingly, our previous work showed that ceramides can induce apoptosis and necrosis in cultured cardiomyocytes by a mechanism involving increased Ca^{2+} influx, mitochondrial network fragmentation and loss of the mitochondrial Ca^{2+} buffer capacity [6]. It is tempting to speculate that ceramide production could be one of the mechanisms by which palmitate induces mitochondrial fission, dysfunction and cell death in our model.

Palmitate, and other saturated fatty acids, are known to induce cell death in several models, including cardiomyocytes [4–6,43] through a mechanism that has not been completely elucidated. Ceramide production has been proposed to mediate palmitate-induced cell death, since ceramides have toxic effects [4,6,43]. We found evidence of both necrosis and apoptosis by palmitate treatment, together with increased ceramide production. However, it is unclear if the increase in cell death was caused specifically by palmitate or ceramides in our conditions, and it has been previously reported that palmitate-induced death can occur independently of the production of ceramides in certain conditions [43].

To date, there is no information relating TMZ to changes in mitochondrial dynamics. We found that TMZ at low concentrations induced marked mitochondrial fusion, without changes in the expression levels of several mitochondrial dynamics proteins assessed. However, it is generally thought that the control of mitochondrial morphology mostly relies on the activity, rather than the mass, of the mitochondria shaping proteins [8,9]. DRP-1 has received most of the attention due to several post-translational modifications described that can regulate its activity as a fission protein [44]. DRP-1 Ser637 phosphorylation is regulated by protein kinase A (PKA) and the phosphatase calcineurin (CN) [38]. Increased Ser637 phosphorylation inactivates DRP-1 and inhibits mitochondrial fission, while dephosphorylation causes the opposite. Herein we describe that TMZ blunts palmitate-induced dephosphorylation of DRP-1 on Ser637. On the one hand, this finding corroborates our immunofluorescence data, further suggesting that palmitate fission occurs through activation of DRP-1; on the other hand, it also provides a novel molecular mechanism for the morphological effects and the protection induced by TMZ. However, determining the specific pathway involved was beyond the scope of this study.

The metabolic effects of TMZ have been extensively studied in different models of hypoxia. It has been described that TMZ decreases the activity of complex I of the mitochondrial electron transport chain [15], decreasing oxygen consumption [45], ROS production [16], and increasing mitochondrial integrity [17], probably by decreasing the opening of the mitochondrial permeability transition pore and subsequent apoptosis [20]. However, our findings point in the opposite direction. We found that TMZ potentiated mitochondrial metabolism, by increasing Ψ_{mt}, OCR, and ATP levels. This seems rather counterintuitive for a drug that should inhibit free fatty acid oxidation in a cell that is highly dependent on β-oxidation. However, it should be considered that in our culture conditions both oxygen and glucose were in abundance for the cells, thus TMZ could generate a metabolic shift and potentiate glucose metabolism through the mitochondrial pathway, accounting for the augmented mitochondrial activity. Interestingly, TMZ has been shown to increase the intra-mitochondrial calcium concentration [46], which could potentiate mitochondrial metabolism and ATP synthesis by favoring the activity of several citric acid cycle dehydrogenases [47]. In fact, in animal models, it has been shown that administration of TMZ increases the mitochondrial affinity for ADP and also the creatine kinase activity. Although MacInnes et al. [22] described that TMZ does not inhibit the 3-CAT enzyme in the heart.

To our surprise, we found a differential effect of TMZ on mitochondrial morphology and function. At low concentration (1 μM) it induced mitochondrial fusion and increased metabolic activity. However, increasing the concentration did not result in augmented effects and mitochondrial morphology and function were comparable to those of control cells at 100 μM TMZ. Although the concentration range tested was in accordance to other studies in the literature [48–50], these results are puzzling and further studies are needed to determine the cause of this difference.

When assessing intracellular destination of lipids in our conditions we found no increase in lipid accumulation in palmitate-treated cells, consistent with the notion that cardiomyocytes have a limited lipid storage capacity. However, in the presence of TMZ, the number and area of lipid droplets was significantly increased in comparison to controls.

There is some evidence that TMZ could inhibit CPT1 [13], thus decreasing the incorporation of free fatty acids to mitochondria at the rate-limiting step of β-oxidation and possibly promoting FFA esterification. Furthermore, a recent clinical trial showed that TMZ promoted glucose oxidation by increasing the rate of muscle FFA esterification in obese patients [51]. Similarly, Bucci et al. [52] described, also in obese patients, that TMZ reduced cardiac free fatty acid oxidation by decreasing the intracellular-derived contribution to total free fatty acid oxidation, without altering the extracellular-derived free fatty acid contribution. These data suggest that TMZ can alter fatty acid utilization in skeletal muscle

(C) Representative immunoprecipation of DRP-1 and Western blot of pDRP-1 (Ser637) on the indicated conditions ($n = 3$). Intracellular ATP levels (D, $n = 6$) and basal (E) and maximal OCR (F, $n = 3$) were determined in Control, TMZ-, palmitate- and TMZ + palmitate-treated cells. Additionally, basal (G) and maximal (H) OCR were determined using a fluorescent probe ($n = 4$) as a secondary method. $^{*}P < 0.05$; $^{**}P < 0.01$; $^{***}P < 0.001$ vs. Control. $^{\#}P < 0.05$; $^{\#\#}P < 0.01$; $^{\#\#\#}P < 0.001$ vs. Palmitate. Tuckey post 1-way ANOVA. Bar graphs represent mean ± SEM.

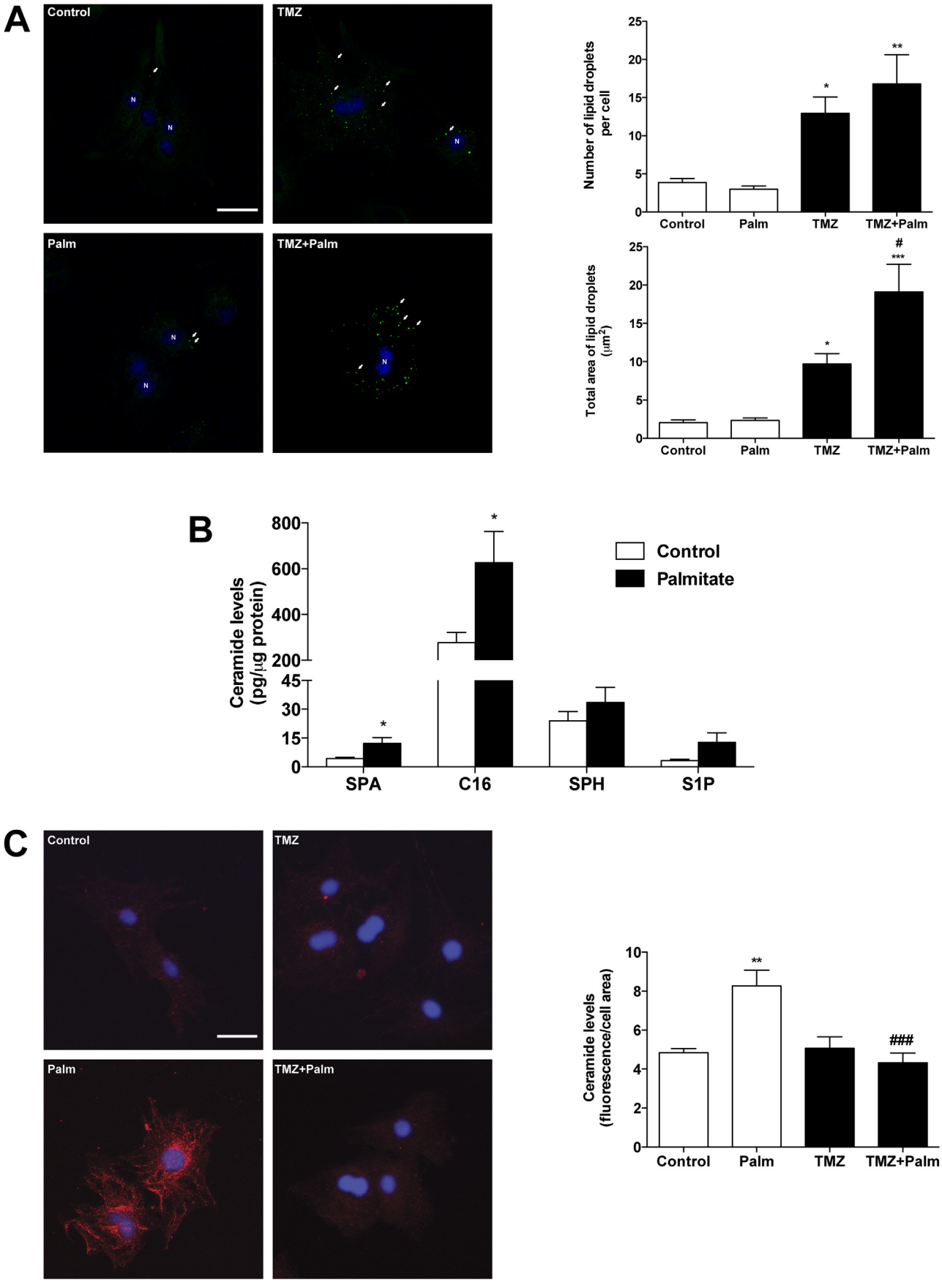

Fig. 8. TMZ increases palmitate accumulation in neutral lipid droplets and blocks palmitate-induced ceramide synthesis. Cells were treated with or without TMZ, palmitate or a combination of both. A, Neutral lipid droplets were stained using LipidTOX and observed under a confocal microscope (left panels). Number of lipid droplets per cell (upper

and heart, supporting our data of increased lipid accumulation. However, it should be noted that neonatal cardiomyocytes could behave very different than adult cardiomyocytes. Nonetheless, evidence of protection by esterification of palmitate excess can be found in other models. In hepatocytes, palmitaoleate increased free fatty acid esterification and protected the cells from palmitate-induced apoptosis [32]. Together, these data argue in favor of the protection from palmitate lipotoxicity induced by the sequestration of palmitate excess in esterified pools.

Over the last decades, changes in mitochondrial morphology have been linked to several cardiovascular and metabolic diseases. However, we still lack an integrated model in which mitochondrial dynamics has been incorporated in normal cardiac physiology. Nonetheless, mitochondrial dynamics are thought to play a crucial role in metabolic flexibility, and there is consensus that the alterations in mitochondrial morphology participate in the progression of cardiovascular diseases [8]. The development of new therapeutic interventions targeted to the manipulation of mitochondrial dynamics could be a relevant contribution to the actual asset for treating these diseases.

Funding

This work was supported by "Comisión Nacional de Investigación Científica y Tecnológica (CONICYT)" grants ANILLO 1111 [to S.L., M.C. and P.C.], FONDAP 15130011 [to S.L., M.C., H.E.V., L.G. and P.F.C.] and FONDECYT [1120212 to S.L and 1090727 to P.C.]. Conicyt scholarship 21130200 (CLC) holds a doctoral scholarship from CONICYT-CHILE. V.P. thanks Conicyt scholarship 74120010 (VP) and the AHA fellowship 13POST16520009 for her postdoctoral funding. DAB is supported by NIH DK084669 and the Minnesota Obesity Center (NIH DK050456).

Conflicts of interests

None declared.

Acknowledgments

We thank Fidel Albornoz and Gindra Latorre for their excellent technical assistance.

References

[1] Wende AR, Abel ED. Lipotoxicity in the heart. Biochim Biophys Acta 2010;1801:311–9.
[2] Lopaschuk GD, Ussher JR, Folmes CD, Jaswal JS, Stanley WC. Myocardial fatty acid metabolism in health and disease. Physiol Rev 2010;90:207–58.
[3] Hickson-Bick DL, Sparagna GC, Buja LM, McMillin JB. Palmitate-induced apoptosis in neonatal cardiomyocytes is not dependent on the generation of ROS. Am J Physiol Heart Circ Physiol 2002;282:H656–64.
[4] Summers SA. Ceramides in insulin resistance and lipotoxicity. Prog Lipid Res 2006;45:42–72.
[5] Parra V, Eisner V, Chiong M, Criollo A, Moraga F, Garcia A, et al. Changes in mitochondrial dynamics during ceramide-induced cardiomyocyte early apoptosis. Cardiovasc Res 2008;77:387–97.
[6] Parra V, Moraga F, Kuzmicic J, Lopez-Crisosto C, Troncoso R, Torrealba N, et al. Calcium and mitochondrial metabolism in ceramide-induced cardiomyocyte death. Biochim Biophys Acta 2013;1832:1334–44.
[7] Dyntar D, Eppenberger-Eberhardt M, Maedler K, Pruschy M, Eppenberger HM, Spinas GA, et al. Glucose and palmitic acid induce degeneration of myofibrils and modulate apoptosis in rat adult cardiomyocytes. Diabetes 2001;50:2105–13.
[8] Kuzmicic J, Del Campo A, Lopez-Crisosto C, Morales PE, Pennanen C, Bravo-Sagua R, et al. Mitochondrial dynamics: a potential new therapeutic target for heart failure. Rev Esp Cardiol 2011;64:916–23.
[9] Parra V, Verdejo H, del Campo A, Pennanen C, Kuzmicic J, Iglewski M, et al. The complex interplay between mitochondrial dynamics and cardiac metabolism. J Bioenerg Biomembr 2011;43:47–51.
[10] Molina AJ, Wikstrom JD, Stiles L, Las G, Mohamed H, Elorza A, et al. Mitochondrial networking protects beta-cells from nutrient-induced apoptosis. Diabetes 2009;58:2303–15.
[11] Jheng HF, Tsai PJ, Guo SM, Kuo LH, Chang CS, Su IJ, et al. Mitochondrial fission contributes to mitochondrial dysfunction and insulin resistance in skeletal muscle. Mol Cell Biol 2012;32:309–19.
[12] Allibardi S, Chierchia SL, Margonato V, Merati G, Neri G, Dell'Antonio G, et al. Effects of trimetazidine on metabolic and functional recovery of postischemic rat hearts. Cardiovasc Drugs Ther 1998;12:543–9.
[13] Hamdan M, Urien S, Le Louet H, Tillement JP, Morin D. Inhibition of mitochondrial carnitine palmitoyltransferase-1 by a trimetazidine derivative, S-15176. Pharmacol Res 2001;44:99–104.
[14] Guarnieri C, Muscari C. Beneficial effects of trimetazidine on mitochondrial function and superoxide production in the cardiac muscle. Cardiovasc Drugs Ther 1990;4(Suppl. 4):814–5.
[15] Veitch K, Maisin L, Hue L. Trimetazidine effects on the damage to mitochondrial functions caused by ischemia and reperfusion. Am J Cardiol 1995;76:25B–30B.
[16] Guarnieri C, Muscari C. Beneficial effects of trimetazidine on mitochondrial function and superoxide production in the cardiac muscle of monocrotaline-treated rats. Biochem Pharmacol 1988;37:4685–8.
[17] Morillas Blasco PJ, Hernandiz Martinez A, Azorin Villena I, Portoles Sanz M, Pallares Carratala V, Martinez VB, et al. Mitochondrial changes induced by trimetazidine in the myocardium. Med Sci Monitor 2005;11:BR162–67.
[18] Monteiro P, Duarte AI, Goncalves LM, Moreno A, Providencia LA. Protective effect of trimetazidine on myocardial mitochondrial function in an ex-vivo model of global myocardial ischemia. Eur J Pharmacol 2004;503:123–8.
[19] Morin D, Elimadi A, Sapena R, Crevat A, Carrupt PA, Testa B, et al. Evidence for the existence of [3H]-trimetazidine binding sites involved in the regulation of the mitochondrial permeability transition pore. Br J Pharmacol 1998;123:1385–94.
[20] Argaud L, Gomez L, Gateau-Roesch O, Couture-Lepetit E, Loufouat J, Robert D, et al. Trimetazidine inhibits mitochondrial permeability transition pore opening and prevents lethal ischemia-reperfusion injury. J Mol Cell Cardiol 2005;39:893–9.
[21] Schrauwen P, Schrauwen-Hinderling V, Hoeks J, Hesselink MK. Mitochondrial dysfunction and lipotoxicity. Biochim Biophys Acta 2010;1801:266–71.
[22] MacInnes A, Fairman DA, Binding P, Rhodes J, Wyatt MJ, Phelan A, et al. The antianginal agent trimetazidine does not exert its functional benefit via inhibition of mitochondrial long-chain 3-ketoacyl coenzyme A thiolase. Circ Res 2003;93:e26–32.
[23] Parra V, Verdejo HE, Iglewski M, Del Campo A, Troncoso R, Jones D, et al. Insulin stimulates mitochondrial fusion and function in cardiomyocytes via the Akt-mTOR-NFkappaB-Opa-1 signaling pathway. Diabetes 2014;63:75–88.
[24] Foncea R, Andersson M, Ketterman A, Blakesley V, Sapag-Hagar M, Sugden PH, et al. Insulin-like growth factor-I rapidly activates multiple signal transduction pathways in cultured rat cardiac myocytes. J Biol Chem 1997;272:19115–24.
[25] van der Lee KA, Vork MM, De Vries JE, Willemsen PH, Glatz JF, Reneman RS, et al. Long-chain fatty acid-induced changes in gene expression in neonatal cardiac myocytes. J Lipid Res 2000;41:41–7.
[26] Richieri GV, Anel A, Kleinfeld AM. Interactions of long-chain fatty acids and albumin: determination of free fatty acid levels using the fluorescent probe ADIFAB. Biochemistry 1993;32:7574–80.
[27] Manders EMM, Verbeek FJ, Aten JA. Measurement of co-localization of objects in dual-colour confocal images. J Microsc 1993;169:375–82.
[28] Pedrozo Z, Torrealba N, Fernandez C, Gatica D, Toro B, Quiroga C, et al. Cardiomyocyte ryanodine receptor degradation by chaperone-mediated autophagy. Cardiovasc Res 2013;98:277–85.
[29] Rotter D, Grinsfelder DB, Parra V, Pedrozo Z, Singh S, Sachan N, et al. Calcineurin and its regulator, RCAN1, confer time-of-day changes in susceptibility of the heart to ischemia/reperfusion. J Mol Cell Cardiol 2014;74C:103–11.
[30] Blachnio-Zabielska AU, Persson XM, Koutsari C, Zabielski P, Jensen MD. A liquid chromatography/tandem mass spectrometry method for measuring the in vivo incorporation of plasma free fatty acids into intramyocellular ceramides in humans. Rapid Commun Mass Spectrom 2012;26:1134–40.
[31] Blachnio-Zabielska AU, Koutsari C, Tchkonia T, Jensen MD. Sphingolipid content of human adipose tissue: relationship to adiponectin and insulin resistance. Obesity 2012;20:2341–7.
[32] Akazawa Y, Cazanave S, Mott JL, Elmi N, Bronk SF, Kohno S, et al. Palmitoleate attenuates palmitate-induced Bim and PUMA up-regulation and hepatocyte lipoapoptosis. J Hepatol 2010;52:586–93.

right panel) and total area of lipid droplets (lower right panel) were quantified ($n = 6$). B, Intracellular sphingolipid content was measured with a mass spectrometer in palmitate treated cells ($n = 4$). C, Sphingosine production was assessed by immunofluorescence and confocal microscopy (left). Total fluorescence was normalized by cell area (right panel, $n = 5$). Nuclei were marked with Hoescht. Scale bar: 10 μm. $^{*}P < 0.05$; $^{**}P < 0.01$; vs. Control. $^{\#}P < 0.05$; $^{\#\#\#}P < 0.001$ vs. Palmitate. Tuckey post 1-way ANOVA. Bar graphs represent mean ± SEM.

[33] Chiong M, Parra V, Eisner V, Ibarra C, Maldonado C, Criollo A, et al. Parallel activation of Ca(2+)-induced survival and death pathways in cardiomyocytes by sorbitol-induced hyperosmotic stress. Apoptosis 2010;15:887–903.
[34] Nicholls DG. Fluorescence measurement of mitochondrial membrane potential changes in cultured cells. Methods Mol Biol 2012;810:119–33.
[35] Brand MD, Nicholls DG. Assessing mitochondrial dysfunction in cells. Biochem J 2011;435:297–312.
[36] del Campo A, Parra V, Vasquez-Trincado C, Gutierrez T, Morales PE, Lopez-Crisosto C, et al. Mitochondrial fragmentation impairs insulin-dependent glucose uptake by modulating Akt activity through mitochondrial Ca2+ uptake. Am J Physiol Endocr Metab 2014;306:E1–3.
[37] Zhang L, Lu Y, Jiang H, Zhang L, Sun A, Zou Y, et al. Additional use of trimetazidine in patients with chronic heart failure: a meta-analysis. J Am Coll Cardiol 2012;59:913–22.
[38] Cereghetti GM, Stangherlin A, Martins de Brito O, Chang CR, Blackstone C, Bernardi P, et al. Dephosphorylation by calcineurin regulates translocation of Drp1 to mitochondria. PNAS 2008;105:15803–08.
[39] Yang C, Aye CC, Li X, Diaz Ramos A, Zorzano A, Mora S. Mitochondrial dysfunction in insulin resistance: differential contributions of chronic insulin and saturated fatty acid exposure in muscle cells. Biosci Rep 2012;32:465–78.
[40] Gwiazda KS, Yang TL, Lin Y, Johnson JD. Effects of palmitate on ER and cytosolic Ca2+ homeostasis in beta-cells. Am J Physiol Endocr Metab 2009;296:E690–701.
[41] Hara T, Mahadevan J, Kanekura K, Hara M, Lu S, Urano F. Calcium efflux from the endoplasmic reticulum leads to beta-cell death. Endocrinology 2014;155:758–68.
[42] Mironova GD, Belosludtsev KN, Belosludtseva NV, Gritsenko EN, Khodorov BI, Saris NE. Mitochondrial Ca2+ cycle mediated by the palmitate-activated cyclosporin A-insensitive pore. J Bioenerg Biomembr 2007;39:167–74.
[43] Listenberger LL, Ory DS, Schaffer JE. Palmitate-induced apoptosis can occur through a ceramide-independent pathway. J Biol Chem 2001;276:14890–95.
[44] Chang CR, Blackstone C. Cyclic AMP-dependent protein kinase phosphorylation of Drp1 regulates its GTPase activity and mitochondrial morphology. J Biol Chem 2007;282:21583–87.
[45] Guarnieri C, Muscari C. Effect of trimetazidine on mitochondrial function and oxidative damage during reperfusion of ischemic hypertrophied rat myocardium. Pharmacology 1993;46:324–31.
[46] Guarnieri C, Finelli C, Zini M, Muscari C. Effects of trimetazidine on the calcium transport and oxidative phosphorylation of isolated rat heart mitochondria. Basic Res Cardiol 1997;92:90–5.
[47] Cardenas C, Miller RA, Smith I, Bui T, Molgo J, Muller M, et al. Essential regulation of cell bioenergetics by constitutive InsP3 receptor Ca2+ transfer to mitochondria. Cell 2010;142:270–83.
[48] Liu F, Yin L, Zhang L, Liu W, Liu J, Wang Y, et al. Trimetazidine improves right ventricular function by increasing miR-21 expression. Int J Mol Med 2012;30:849–55.
[49] Wu Q, Qi B, Liu Y, Cheng B, Liu L, Li Y, et al. Mechanisms underlying protective effects of trimetazidine on endothelial progenitor cells biological functions against H2O2-induced injury: involvement of antioxidation and Akt/eNOS signaling pathways. Eur J Pharmacol 2013;707:87–94.
[50] Ferraro E, Giammarioli AM, Caldarola S, Lista P, Feraco A, Tinari A, et al. The metabolic modulator trimetazidine triggers autophagy and counteracts stress-induced atrophy in skeletal muscle myotubes. FEBS J 2013;280:5094–108.
[51] Bucci M, Borra R, Nagren K, Maggio R, Tuunanen H, Oikonen V, et al. Human obesity is characterized by defective fat storage and enhanced muscle fatty acid oxidation, and trimetazidine gradually counteracts these abnormalities. Am J Physiol Endocr Metab 2011;301:E105–12.
[52] Bucci M, Borra R, Nagren K, Parkka JP, Del Ry S, Maggio R, et al. Trimetazidine reduces endogenous free fatty acid oxidation and improves myocardial efficiency in obese humans. Cardiovasc Ther 2012;30:333–41.